Real-Time Monitoring of P-Glycoprotein Activation in Living Cells†

Ewa Landwojtowicz, Pierluigi Nervi, and Anna Seelig*

Division of Biophysical Chemistry, Biozentrum, University of Basel, Klingelbergstrasse 70, Switzerland

Received February 22, 2002; Revised Manuscript Received April 19, 2002

ABSTRACT: Extracellular acidification rates (ECARs) in response to eight different drugs activating or inhibiting the ATPase of P-glycoprotein (Pgp) were measured in real time by means of a Cytosensor microphysiometer in MDR1-transfected and corresponding wild-type cell lines, i.e., pig kidney cells (LLC-MDR1 and LLC-PK1) and mouse embryo fibroblasts (NIH-MDR-G185 and NIH3T3). The ECARs showed a bell-shaped dependence on drug concentration (log scale) in transfected cells but were negligibly small in wild-type cells. The activation profiles (ECARs vs concentration) were analyzed in terms of a model assuming activation of Pgp-ATPase with one and inhibition with two drug molecules bound. The kinetic constants [concentration of half-maximum activation (inhibition), K_i, and the maximum (minimum) transporter activity, V_i] were in qualitative and quantitative agreement with those determined earlier for Pgp-ATPase activation monitored by phosphate release in inside-out cellular vesicles and in purified reconstituted systems, respectively. Furthermore, the ECARs correlated with the expression level of Pgp in the two different cell lines and were reduced in a concentration-dependent manner by cyclosporin A, a potent inhibitor of the Pgp-ATPase. In contrast, treatment of cells with inhibitors of the Na^+/H^+ or the Cl^-/HCO_3^- exchanger did not reduce the ECARs. The micro-pH measurements provide for the first time direct evidence for a tight coupling between the rate of extracellular proton extrusion and intracellular phosphate release upon Pgp-ATPase activation. They support a Pgp-mediated transport of protons from the site of ATP hydrolysis to the cell surface. Measurement of the ECARs could thus constitute a new method to conveniently analyze the kinetics of Pgp-ATPase activation in living cells.

P-glycoprotein (Pgp),[1] an ATP binding cassette (ABC) transporter, extrudes a wide variety of endogeneous and exogeneous compounds out of the cell (for review cf. refs *1*−*4*). Pgp is expressed at high levels in tissues with protective functions, such as the apical surface of the intestinal epithelium or the endothelium of the blood capillaries in the brain, i.e., the blood−brain barrier. It is also expressed at high levels in cancer cells to which it confers multidrug resistance. The transporter has a molecular weight of 170 kDa and comprises two nucleotide-binding and two membrane-spanning domains. On the basis of hydropathy plots, each of the membrane spanning domains have been proposed to consist of six transmembrane α-helices. The six-transmembrane motif has been confirmed by X-ray crystallography for a related homologous bacterial MDR−ABC transporter, MsbA (*5*). Pgp has been proposed to access its substrates in the lipid bilayer (*6*). Recently, partitioning of substrates into the bilayer has been shown to be a prerequisite for substrate−Pgp interaction (*7*, *8*). Fluorescence measurements provided evidence for translocation of the substrate from the inner to the outer membrane leaflet (*9*) or to the aqueous extracellular environment (*10*).

Substrates for Pgp are chemically very diverse. However, they share specific hydrogen bond acceptor patterns that may be recognized by hydrogen bond donor side chains arranged in an amphipatic manner in the putative transmembrane helices of Pgp (*11*, *12*). The drug extrusion cycle of Pgp was proposed to include two ATP hydrolysis steps, the first required to induce the drug-releasing conformation and the second to reset the transporter to the drug-binding conformation (*13*). Pgp displays constitutive ATPase activity in the absence of exogeneous substrates in inside-out cellular vesicles (*14*−*16*) and when reconstituted in proteoliposomes (*17*). Whether basal activity arises from uncoupled ATPase activity (*18*) or whether it is due to the transport of endogeneous substrates is not yet fully clarified. In reconstituted systems, the most likely endogeneous substrates are membrane lipids (*19*, for review see ref *20*). In intact cells, further endogeneous substrates may be present.

Pgp-ATPase activation was observed to cause a cytosolic alcalinization in cells overexpressing Pgp (*21*−*24*). This increased cytosolic pH was suggested to correlate with a low extracellular pH which could decrease the accumulation of weak bases and positively charged drugs in the cytosol (*25*). For basal conditions (i.e., no drug activation), maintenance and regulation of intracellular pH was extensively studied in wild-type Ehrlich ascite tumor cells and five progressively daunorubicin-resistant strains, expressing Pgp at different levels (*26*). Evidence was provided for a constant cytosolic pH under steady-state conditions, which was independent of the expression level of Pgp. This observation was

† Supported by the Swiss National Science Foundation Grant No. 31-58800.99.

* Corresponding author: Phone: +41-61.267 22 06. Fax: +41-61-267-2189. E-mail: Anna.Seelig@unibas.ch.

[1] Abbreviations: LLC-PK1, and LLC-MDR1, wild type and transfected pig kidney epithelial cells; NIH3T3, and NIH-MDR-G185, wild type and transfected mouse embryo fibroblasts; ECAR, extracellular acidification rate.

10.1021/bi025720s CCC: $22.00
Published on Web 06/04/2002

confirmed recently (*27*). As far as the extracellular milieu is concerned, findings are controversial. On one hand, resistant cells exhibiting reduced steady-state drug accumulation and increased drug efflux were shown to have no effect in local extracellular pH (*28*). On the other hand, an ATP-dependent proton transport mediated by Pgp has been suggested resulting in extracellular acidification (*29*).

The aim of the present investigation therefore was to examine whether a stimulation of living cells with drugs known to activate the Pgp-ATPase changes the extracellular pH. To this purpose, we used a pH microsensor that detects the rate of excretion of acidic metabolic products of living cells with a pH-sensitive silicon wafer (*30*, *31*). To test the ATPase specificity of the extracellular acidification, we compared the response of cells transfected with the human MDR1 (multidrug resistance) gene, overexpressing Pgp, with that of wild-type (wt) cells, exhibiting only a low level of Pgp. We measured the concentration-dependent response to eight different drugs interacting with the Pgp-ATPase (amitriptyline, calcein-AM, cyclosporin A, diltiazem, progesterone, trifluoperazine, verapamil, and vinblastine) in pig kidney epithelial cells (LLC-PK1 and LLC-MDR1). Furthermore, we tested the effect of verapamil in a second cell line, i.e., mouse embryo fibroblasts (NIH3T3 and NIH-MDR-G185). The kinetics of the Pgp-ATPase related pH changes at the surface of transfected cells was then compared with earlier phosphate release measurements of inside-out membrane vesicles (*15*, *32*, *33*). The pH response was also measured in the presence of the Pgp-ATPase inhibitor cyclosporin A. Furthermore, the Na^+/H^+ and the Cl^-/HCO_3^- exchanger, both major regulators of intracellular pH in mammalian cells, were inhibited during drug stimulation to test their potential contributions to the extracellular acidification rate (ECAR).

We showed that the drug-induced changes in ECARs in MDR1-transfected cells are specific for Pgp-ATPase activation. They parallel the changes in the rate of phosphate release upon drug stimulated Pgp-ATPase activation in inside-out cellular vesicles, and can be described quantitatively by the same kinetic model as the drug-induced release of inorganic phosphate. The analysis of the ECARs provides direct evidence for a coupled release of phosphate to the cytosol and protons to the cell surface upon ATP hydrolysis and helps to clarify previous conflicting results.

MATERIAL AND METHODS

Compounds. Amiloride, 5,5-(*N*-dimethyl)-amiloride (DMA), diltiazem, progesterone, trifluoperazine, (R/S) verapamil, and vinblastine were purchased from Sigma (Steinheim, Germany); calcein acetoxymethyl ester (calcein-AM) was from Molecular Probes (Leiden, The Netherlands); and 2-deoxy-D-glucose was from Fluka (Switzerland). Amitriptyline and cyclosporin A were gifts from Merck (Darmstadt, Germany) and Novartis (Basel, Switzerland), respectively. For stock solutions cyclosporin A, vinblastine, and calcein-AM were dissolved in DMSO, and progesterone was dissolved in ethanol. Solvent concentrations in the final solutions were $\leq$0.5%. The other compounds were directly dissolved in medium (see below). Anti-P-glycoprotein, clone MRK16, and unspecific antibody, IgG_{2ak}, were from Kamiya Biomedical Company (Seattle, USA), and the IgG_{2a} FITC-labeled antibody was from PharMingen (San Diego, USA). Cell culture media, M199 (Cat. No. 31153) used for LLC-PK1 and LLC-MDR1 cells, DMEM (Cat. No. 21969) used for NIH3T3 and NIH-MDR-G185 cells, and IMDM (Cat. No. 21056) used for FACS analysis of both cell types were from Gibco-BRL (Basel, Switzerland), as well as additional compounds required for cell culture such as fetal bovine serum (FBS), bovine serum albumin (BSA), and antibiotics. For cytosensor measurements, a flow medium with low buffer capacity is required. The flow medium was prepared from commercially available dry powder MEM (Cat. No. 61100). To reduce the buffer capacity of the medium but nevertheless preserve the osmotic balance, $NaHCO_3$ (26.4 mM in MEM) was replaced by NaCl (26.4 mM). The flow medium further contained NaH_2PO_4 (1 mM) and was adjusted to pH 7.4. The osmolality of the flow medium was very similar to that of the culture medium.

Cell Lines. The pig kidney polarized epithelial cell lines, LLC-PK1 (wt) and LLC-PK1 transfected with the human MDR1 gene (LLC-MDR1) (selected with 0.64 μM vincristine) (*34*) and the mouse embryo fibroblast cell lines NIH3T3 and NIH3T3 transfected with the human MDR1 gene (NIH-MDR-G185) (selected with 0.15 μM colchicine) (*35*) were generously provided by Dr. P. Borst (The Netherlands Cancer Institute, Amsterdam, The Netherlands) and Dr. M. M. Gottesman (The National Institutes of Health, Bethesda, USA), respectively.

Cell Culture. Cells were maintained under standard cell culture conditions. Pig kidney cells were grown in the absence of vincristine in monolayer culture (*34*). Vincristine was omitted to avoid the development of other drug resistance mechanisms that could modify the action of Pgp (*36*). The Pgp level in LLC-MDR cells was tested by a calcein-AM assay (*37*) and was stable up to at least 10 passages. Mouse fibroblasts were grown in the presence of colchicine as described previously (*35*).

Detection of Pgp Expression. The expression level of Pgp in wt (LLC−PK1 and NIH3T3) and transfected cells (LLC-MDR1 and NIH-MDR-G185) was estimated using the monoclonal antibody, MRK16, which recognizes only human Pgp. Aliquots of $2-3 \times 10^5$ cells were incubated in IMDM containing 5% FBS at 37 °C for 30 min in the presence of MRK16 or the unspecific antibody IgG_{2ak}. After the cells were washed, they were reincubated at 37 °C for 30 min in the dark, in the presence of FITC-labeled antibody. Cells were resuspended in phosphate buffered saline (containing 1% BSA), and FACS analysis was performed. LLC-MDR1 and NIH-MDR-G185 cells expressed detectable levels of Pgp, but wt cells (LLC-PK1 and NIH3T3) lacking the human MDR1 gene did not.

Cytosensor Measurements. ECARs of intact cells were measured with a Cytosensor microphysiometer (Molecular Devices, Menlo Park, CA) described in detail elsewhere (*31*). In short, the instrument consists of a parallel set of four or eight light-addressable potentiometric sensors that are in diffusive contact with a cell layer grown on a polycarbonate membrane which forms the bottom of a flow chamber. The light-addressable potentiometric sensors make a voltage measurement each second that is linearly related to pH. According to the calibration made, 58.9 mV corresponded to 1 pH unit. The cytosensor detects micro-pH changes in the extracellular fluid of cells in the flow chamber (*38*). The internal size of the flow chamber is defined by the volume

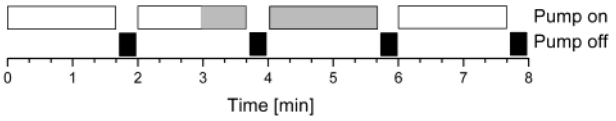

FIGURE 1: Pump cycles for stimulation of P-glycoprotein with drugs. During each 2-min pump cycle, the pump was on for 1 min 40 s and was then switched off for the remaining 20 s. During the pump-off period of 13 s (from 1:45 to 1:58 min) (black bars) in each pump cycle, the acidification rate of the extracellular medium in the sensor chamber is determined. During the pump-on period of 1 min 40 s, cells were first superfused with a drug-free medium (white bars). After a constant acidification rate was reached, the medium was replaced by a drug-containing medium (gray bars) for 40 s. Drug superfusion was continued for a further two minutes. Finally, the drug-containing medium was switched back to a drug-free medium.

entrapped between the bottom and the cover polycarbonate membrane separated by a plastic spacer ring with the height of 50 μm and an inner diameter of 6 mm placed directly on the cell layer between the two polycarbonate membranes (1.4 μL). After the capsule cup is inserted into the sensor chamber, a fluid delivering plunger is placed into the capsule cup, creating a flow chamber of 2.8 μL. A computer controls the pumps for delivery of medium to the chambers, the switching valves, the temperature of the sensor chambers, and the acquisition of data (for details see ref *30*).

Cells were seeded at a density of $1-4 \times 10^5$ cells per cup in the culture medium with 10% FBS and were kept at 37 °C for ~15 h to allow for recovery and attachment to the polycarbonate membrane. The number of cells in the measuring chamber is smaller and corresponds to ~25% of the cells seeded. For pH measurements, the culture medium was replaced by flow medium which was pumped at a constant rate (100 μL/min or ~0.5 volume shifts per second) from the primary fluid reservoir into the chambers at an on−off cycle according to the flowchart shown in Figure 1. A constant acidification rate was reached about 60−70 min after the replacement of the culture medium by the flow medium. At the beginning of a measurement, the pH of the solution was always adjusted to 7.4.

The optimal drug stimulation time was determined by measuring the ECARs as a function of drug-stimulation time (6−220 s) (not shown). At drug stimulation times $t > 150$ s, a steady state was reached for all drugs investigated. Data for the kinetic analyses were therefore collected at a drug stimulation time of 160 s.

Quantification of Proton Release. Since cells excrete protons into buffered solutions and potentiometric methods detect pH changes rather than $[H^+]$ directly, it is important to establish the relationship between the number of protons excreted into a volume V, the resulting pH change. The number of protons excreted was calculated according to (*39*):

$$\beta \equiv -\frac{\mathrm{d}(n/V)}{\mathrm{dpH}} = \ln(10) A_{\mathrm{tot}} \frac{10^{(\mathrm{pK}-\mathrm{pH})}}{(1+10^{(\mathrm{pK}-\mathrm{pH})})^2} \qquad (1)$$

where β is the buffer capacity, n is the number of protons excreted into the volume V, dpH is the pH change measured, and A_{tot} is the buffer concentration. With a 1 mM phosphate buffer at pH 7.4 and a pK_a 6.76 (second pK_a at $T = 310$ K) (*40*) the buffer capacity is calculated as $\beta = 0.35$ mM.

Kinetic Model. A modified Michaelis-Menten equation assuming activation with one substrate molecule, S, and inhibition with two substrate molecules bound to the Pgp transporter, T, was used for the evaluation of the ECARs. The model has been applied previously to describe the release of inorganic phosphate upon Pgp activation (*15*, *33*). The reaction is described in the following scheme:

$$\begin{array}{l} \mathrm{T + ATP + S} \underset{k_{-1}}{\overset{k_1}{\rightleftharpoons}} \mathrm{T(ATP)S + S} \xrightarrow{k_2} \mathrm{T(ATP)S_2} \xrightarrow{k''} \mathrm{T(ADP) + 2S_{rel} + P_i + H^+} \\ \qquad\qquad\qquad\qquad\qquad\qquad \downarrow k' \\ \qquad\qquad\qquad\qquad\qquad\qquad \mathrm{T(ADP) + P_i + H^+ + S_{rel}} \end{array} \qquad (2)$$

T(ATP)S and T(ATP)S_2 are transporter−ATP complexes with one and two substrate molecules bound, respectively, T(ADP) is the transporter−ADP complex, P_i is the inorganic phosphate released intracellularly, and S_{rel} is the substrate molecule released extracellularly.

The corresponding rate equation for the hydrolysis of ATP upon Pgp activation originally derived for P_i release is therefore identical for H^+ release according to the above scheme and can be written as

$$V_{(\mathrm{Saq})} = \frac{K_1 K_2 V_0 + K_2 V_1 C_{\mathrm{Saq}} + V_2 C_{\mathrm{Saq}}^{\ 2}}{K_1 K_2 + K_2 C_{\mathrm{Saq}} + C_{\mathrm{Saq}}^{\ 2}} \qquad (3)$$

where $V_{(\mathrm{Saq})}$ is the ECAR as a function of the substrate concentration in solution, C_{Saq}, V_0 is the basal activity in the absence of substrate, V_1 is the maximum transporter activity (if only activation occurred), and V_2 is the activity at infinite substrate concentration. The maximum and minimum rates of release are

$$V_1 = k' C_{\mathrm{T}}^0 \qquad (4)$$

$$V_2 = k'' C_{\mathrm{T}}^0 \qquad (5)$$

where C_{T}^0 is the total transporter concentration. At low substrate concentration, the monosubstrate complex T(ATP)S is favored, which rapidly releases its substrate with a rate constant k'. At high substrate concentrations, the two-substrate intermediate T(ATP)S_2 is favored. Under these conditions, the release of substrates is slow and the rate constant is k''.

In terms of the above model (eq 2), the parameters K_1 and K_2 have the dimensions of dissociation constants and are given by

$$K_1 = \frac{k_{-1} + k_2 + k'}{k_1} \qquad (6)$$

$$K_2 = \frac{k''}{k_2} \qquad (7)$$

K_1 is the substrate concentration that gives half-maximum activation, and K_2 is the substrate concentration that gives half-maximum reduction of the ECAR from the maximum activity V_1. At low substrate concentrations, where the formation of the T(ATP)S_2 complex can be neglected, K_1 is the classical Michaelis−Menten constant for the one-substrate Pgp reaction, and half-maximum activation is achieved for $C_{\mathrm{Saq}} = K_1$.

RESULTS

Pgp Substrates Induce Changes in the ECAR of MDR1-Transfected but not of Wild-Type Cell Lines. In a first set of

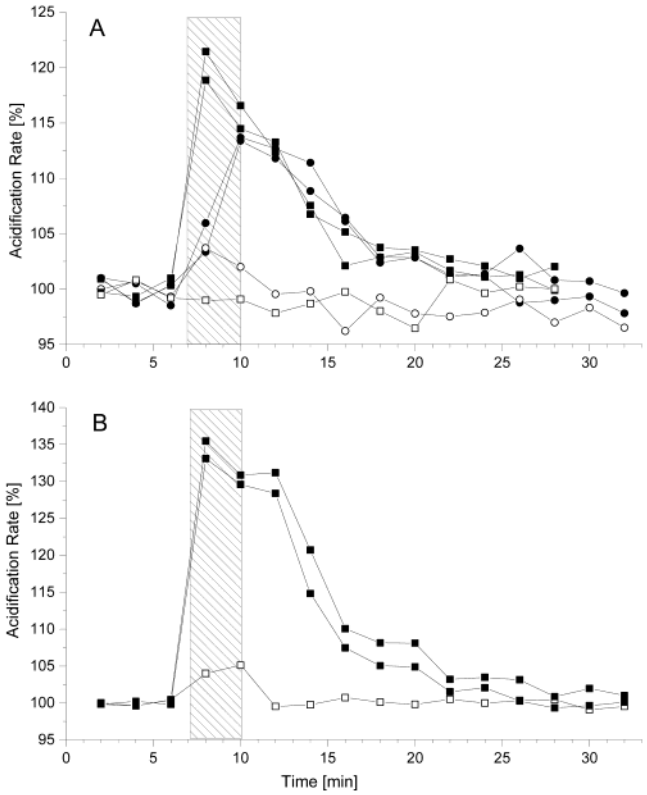

FIGURE 2: Extracellular acidification rates (ECARs) induced by verapamil (■, □) and trifluoperazine (●, ○) (both 10 μM) as a function of time for wild-type (open symbols, one experiment per drug shown) and transfected cells (solid symbols, two experiments per drug shown). (A) LLC−PK1 and LLC-MDR1 cells. (B) NIH3T3 and NIH-MDR-G185. The basal ECAR of cells was defined as 100%. Results are normalized to the baseline and expressed as % of the basal rate. The drug-stimulation period is indicated by hatched bars.

experiments, the basal metabolic rates of cells were measured by determining ECARs in the absence of drugs (cf. Materials and Methods). At 58.9 mV per pH unit, the basal ECAR for a sample of 1×10^5 cells (where ~25% of cells are included in the sensor chamber) was determined as 0.848 ± 0.4 mpH units/s (50 ± 23 ($-\mu$V/s) for LLC-MDR1 cells ($n = 47$ measurements, made with 16 different cell preparations) and 0.559 ± 0.10 mpH units/s (33 ± 6 ($-\mu$V/s)) for NIH-MDR-G185 cells ($n = 4$). Taking into account the buffer capacity β (eq 1), the basal ECAR was calculated as $(1.9 \pm 0.9) \times 10^7$ H^+ s^{-1} $cell^{-1}$ for LLC-MDR1 cells and $(1.3 \pm 0.2) \times 10^7$ H^+ s^{-1} $cell^{-1}$ for NIH-MDR-G185 cells. This value is a lower limit since the buffer capacity of other components

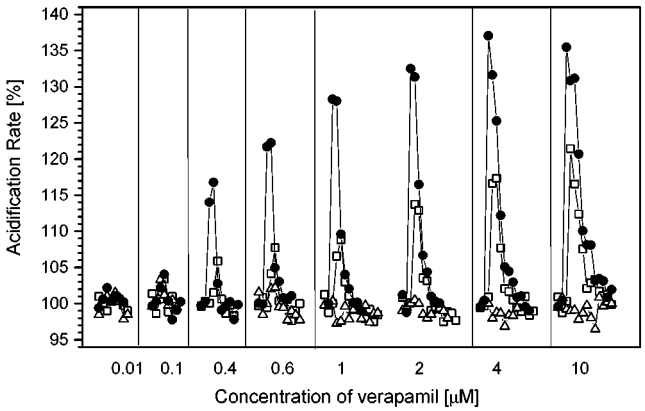

FIGURE 3: ECARs of LLC-PK1 wild-type cells (△) and LLC-MDR1 (□) and NIH-MDR-G185 (●) cells overexpressing Pgp, measured as a function of time upon increasing concentration of verapamil.

of the flow medium (e.g., amino acids) has not been taken into account. A net rate of $\sim 1 \times 10^8$ H^+ s^{-1} $cell^{-1}$ was calculated previously for other cell lines (*31*). For the following measurements, the basal ECAR was defined as 100% (first three sets of points shown in Figure 1), and the change of the ECAR upon drug stimulation was determined relative to the basal value.

Figure 1 shows the time dependence of the ECARs of LLC-PK1 cells and LLC-MDR1 cells stimulated with verapamil and trifluoperazine (10 μM each). The pig kidney cells were superfused for 40 s with a drug-containing medium resulting in a rapid rise of the ECAR. Drug superfusion was continued for two further minutes. For verapamil, the ECAR reaches a maximum at about 120% of the basal rate after 40 s. For trifluoperazine, the ECAR reaches a 113% maximum after 160 s only. After the 2-min stimulation, cells were again superfused with drug-free medium, and the ECAR gradually decreased and reached basal values after approximately 30 min. For wt cells, the response to the same drug stimuli was negligibly small (<104%) (open symbols in Figure 2), providing the first evidence that extracellular acidification of transfected cells is indeed caused by Pgp activation.

The Pgp specificity of the ECAR was tested further in a second transfected cell line. Figure 2B shows a stimulation of wild-type (NIH3T3) and MDR1-transfected (NIH-MDR-G185) mouse fibroblasts with verapamil (10 μM) as a function of time. The kinetics of the acidification response was qualitatively very similar to that in the kidney cell line. However, the ECAR was higher in NIH-MDR-G185 than in LLC-MDR1 cells. This is also seen in Figure 3 which

Table 1: Kinetic Parameters Derived from ECAR Measurements of Intact MDR1-Transfected Cells and Previous Phosphate Release Measurements from Inside-Out Membrane Vesicles

no.	substrate	M_W [g/mol]	V_1^a [fold]	V_2^a [fold]	K_1^a [μM]	K_2^a [μM]	V_1^b [fold]	V_2^b [fold]	K_1^b [μM]	K_2^b [μM]
1	amitriptyline	277.4	1.47	0.84	80	400	2.3	0.9	108	110
2	calcein−AM	994.87	0.89	1.07	0.11	0.4	1.4[d]		0.12[d]	
3	cyclosporin A	1202.6	1.02	0.90	0.03	2	1.06	0.6	0.06	1.7
4	diltiazem	414.5	1.45	0.8	25	190	3.3	0	73.3	677
5	progesterone	314.5	1.41	0.6	17	200	2.6	0.3	17.5	294
6	trifluoperazine	407.50	1.33	0.70	12	100	2.0	0.6	6.5	24.1
7	R/S−verapamil	454.6	1.23	0.88	1.5	100	2.1	0.6	2.5	98.5
			1.37[c]	0.86[c]	0.5[c]	85[c]				
8	vinblastine	811	1.11	0.97	7	55	1.5	0.5	1.3	17.3

[a] Measurements of ECARs of LLC-MDR1 cells. [b] Data taken from ref *15*. [c] Measurements of ECARs of NIH/G185 cells; the constants K_i and V_i (error limit ≤ 20%) are derived from data in Figure 4. [d] Data taken from ref *53*.

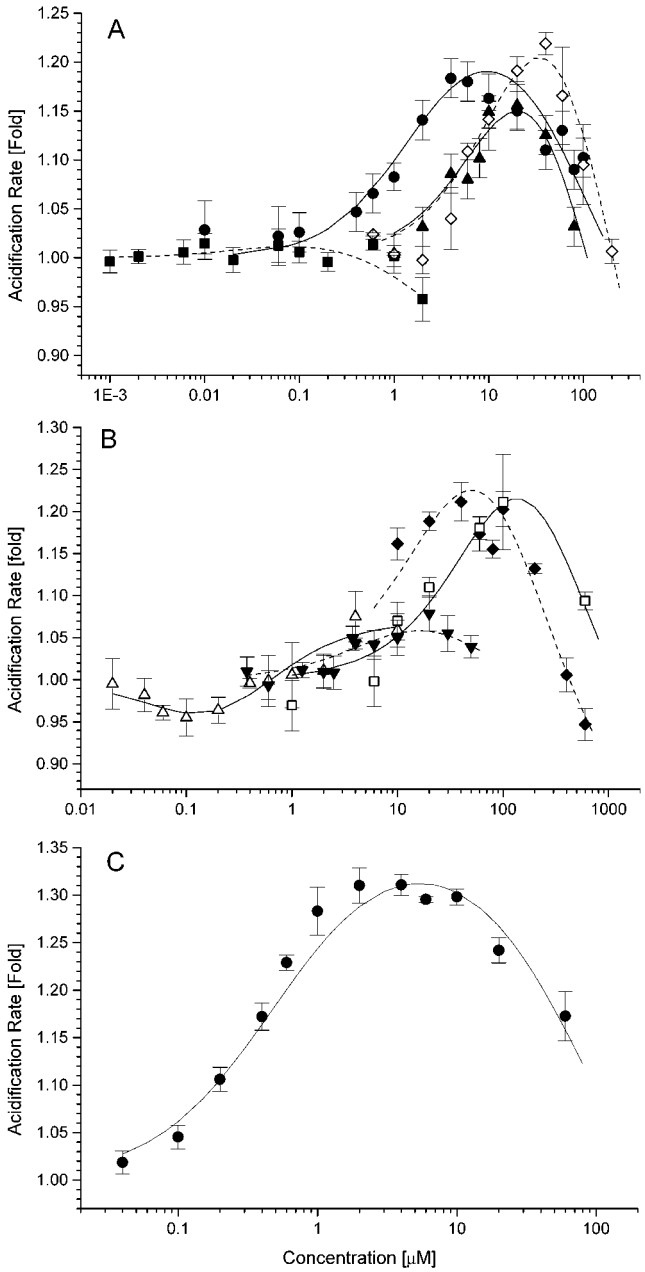

FIGURE 4: Pgp-ATPase activation profiles obtained by measurements of ECARs in living cells: cyclosporin A (■), progesterone (◇), trifluoperazine (▲), and verapamil (●) in LLC-MDR1 cells (A); amitriptylin (□), calcein-AM (△), diltiazem (◆) and vinblastine (▼) in LLC-MDR1 cells (B); and verapamil (●) in NIH-MDR-G185 cells (C). The solid or dashed lines correspond to modified Michaelis−Menten kinetics assuming activation with one and inhibition with two molecules bound according to eq 3 (Materials and Methods). Solid symbols represent an average value of $n = 3-5$ parallel measurements made with one single cell preparation.

shows the ECARs as a function of time upon increasing concentrations of verapamil for pig kidney and mouse fibroblast cells. Verapamil-induced stimulation of extracellular acidification is detectable at concentrations as low as 0.02 μM (not shown) for both cell lines. The ECARs increase in a nonlinear fashion with increasing drug concentration. The response elicited in wt cells is again within error limits and is negligible.

Figure 4A,B shows the ECARs measured at the end of the drug-stimulation period (160 s) as a function of drug concentration (logarithmic scale) for all compounds investigated in LLC-MDR1 cells. The data points are the average of 3−5 measurements. All activation profiles have a bell-shaped apparence. For amitriptyline, diltiazem, progesterone, trifluoperazine, verapamil, and vinblastine, the ECAR increases at low drug concentrations, reaches an apparent saturation, and decreases at high concentrations. For cyclosporin A, the ECAR falls below basal values already at low concentrations. Calcein-AM shows a slight inhibition at low concentration (0.02−0.1 μM) and an activation at higher concentration. The ECARs due to drug stimulation are expressed in units of the basal ECARs. The solid and dashed lines are theoretical fits using eq 3. This multiparameter fit is facilitated by the fact that K_1 corresponds to a concentration that is slightly higher than the concentration at the apparent half-maximum velocity, and V_1 is slightly higher than the apparent maximum velocity. The binding parameters and the kinetic constants (K_1, K_2, V_1, and V_2) are listed in the Table 1. The ECARs elicited in NIH-MDR-G185 cells by increasing concentrations of verapamil are included in Figure 4C.

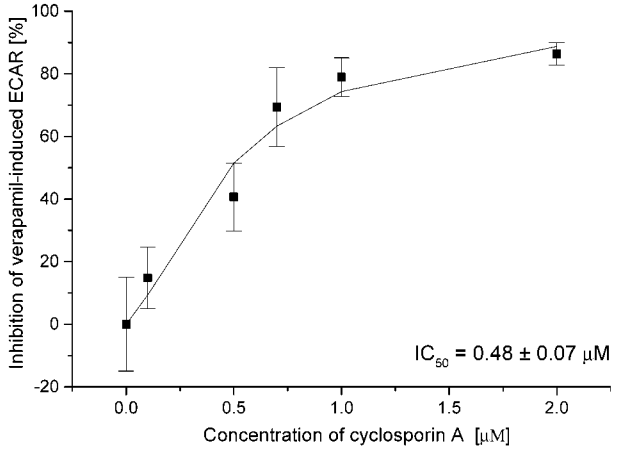

FIGURE 5: Inhibition [%] of the verapamil (1 μM)-induced ECAR by increasing concentrations of cylosporin A.

The Extracellular Acidification Rate is Proportional to the Level of Pgp Expression. Figure 3 shows the ECARs as a function of verapamil concentration in both cell lines measured. For LLC-MDR1 and NIH-MDR-G185 cells, the maximum ECARs, V_1, were 23 and 37% over basal values, respectively, yielding a V_1 ratio (NIH-MDR-G185/LLC-MDR1) $\approx$ 1.6 (cf. Table 1). Pgp expression in the two cell lines was estimated by means of a FACS analysis, and an expression ratio (NIH-MDR-G185/LLC-MDR1) $\approx$ 1.6 was obtained. The higher ECARs of mouse fibroblasts can thus be traced back to the higher expression level of Pgp in this cell line. The data suggest a direct correlation between Pgp expression and the ECAR.

Cyclosporin A, an Inhibitor of the Pgp-ATPase, Reduces the Drug-Induced ECARs in a Concentration-Dependent Manner. If drug-induced ECARs are Pgp-specific, they should be inhibited by cyclosporin A, a potent inhibitor of the Pgp-ATPase (*41*). NIH-MDR-G185 cells were therefore preincubated with cyclosporin A for 20 min and were then stimulated with verapamil (1 μM) in the presence of cyclosporin A.

Figure 5 displays the inhibition of the verapamil-induced ECAR as a function of the concentration of cyclosporin A (0.1−2 μM). The concentration of half-maximum inhibition

is $IC_{50} = 0.47 \pm 0.07$ μM. Similar inhibition values were obtained with LLC-MDR1 cells (not shown). For the same pair of modulators (verapamil as a fixed and cyclosporin A as a variable modulator), a $K_m = 0.58 \pm 0.26$ μM was determined from daunomycin accumulation experiments (*42*). These data thus further confirm the Pgp-specificity of the drug-induced ECARs in transfected cells.

Contributions from the Na^+/H^+ Exchanger and the Cl^-/HCO_3^- Exchanger to the ECAR. In mammalian cells, the Na^+/H^+ and the Cl^-/HCO_3^- exchanger are major regulators of intracellular pH. We therefore investigated their effect on the basal ECAR as well as on the Pgp-related ECAR. Amiloride hydrochloride and DMA (an even more potent and selective analogue of amiloride) were used to inhibit the Na^+/H^+ exchanger. 4,4′-Diisothiocyano-2,2′-disulfonic acid stilbene (DIDS) was employed to inhibit the Cl^-/HCO_3^- exchanger. While amiloride and DMA had no effect on the basal ECAR of LLC-MDR1 and NIH-MDR-G185, DIDS decreased the basal ECAR in both cell lines by about 20%.

To see whether the Na^+/H^+ exchanger and/or the Cl^-/HCO_3^- exchanger contributed to the Pgp-related ECARs in transfected cells, LLC-MDR1 and NIH-MDR-G185 cells were preincubated for 20 min with amiloride (100 μM), DMA (10 μM) or DIDS (200 μM) and were then stimulated with trifluoperazine and verapamil (10 μM) in the presence of the corresponding inhibitors [amiloride (100 μM), DMA (10 μM) or DIDS (200 μM)]. Neither amiloride, DMA, nor DIDS reduced the Pgp-related ECAR. In fact, even a slight increase was observed for DIDS. Protons released at the surface of MDR1-transfected cells are thus not transported via the Na^+/H^+ or the Cl^-/HCO_3^- exchanger. The Na^+/H^+ exchanger was shown previously to have no influence on proton efflux in transfected cell lines (*26*, *43*, *44*), which is in agreement with the present results.

DISCUSSION

Drug-induced activation of the Pgp-ATPase is usually determined by monitoring phosphate release from inside-out membrane vesicles of cells transfected with the human MDR1 gene (*14*, *15*) or from reconstituted proteoliposomes containing purified Pgp (*17*). The present data demonstrate for intact cells that this process is accompanied by minute pH changes at the outer cell surface. Using living MDR1-transfected cells in a supported, nonconfluent cell monolayer of $1-4 \times 10^5$ cells, the ECAR can be measured with high precision in a microphysiometer. The recorded ECARs for two different cell lines (LLC-MDR1 and NIH-MDR-G185) bear close resemblance to the Pgp-ATPase activation profiles determined previously by phosphate release from inside-out membrane vesicles of CR1R12 Chinese hamster ovary cells (*15*). Furthermore, the Pgp-substrate induced ECARs are correlated with the expression level of Pgp, and can be inhibited by cyclosporin A, an inhibitor of the Pgp-ATPase, in a concentration-dependent manner. Measurement of the ECARs could thus constitute a new method to conveniently analyze the Pgp-ATPase activation kinetics in intact cells. In the following, we will discuss the correlation between proton extrusion and Pgp substrate induced ATP hydrolysis in more detail and will then discuss possible mechanisms for proton extrusion via Pgp.

Direct Correlation between Extracellular Acidification Rates and Rates of Phosphate Release upon Pgp-ATPase Activation. The experimental ECARs were analyzed in terms of the model proposed by Litman et al. (*32*) for phosphate release (cf. eq 3). Applying this model to the activation profiles shown in Figure 4 provides the activation constant K_1, the inhibition constant K_2, and the rate parameters V_1 and V_2 (given as fold of basal values). The results of the present analysis are compared with those obtained previously by phosphate release measurements (*15*) (Table 1). The concentrations of half-maximum activation K_1 vary by more than 3 orders of magnitude for the different substrates as seen in Figure 6A; nevertheless, they are in good agreement for the two types of methods and the two different cell lines. A linear correlation is also found for the corresponding maximum velocities, V_1 (Figure 6B). However, the maximum velocities of CR1R12 cells are consistently higher by a factor of ~1.5 than those of LLC-MDR1 cells, and V_2 values are lower by a factor of ~0.65. A similar difference was observed between NIH-MDR-G185 cells and LLC-MDR1 cells. The model described above (cf. eqs 4 and 5) predicts that the rate parameters V_i should be linearly proportional to the concentration of Pgp in the membrane. We have measured the expression level of Pgp for the two cell lines by FACS analysis and found a Pgp ratio (NIH-MDR-G185/

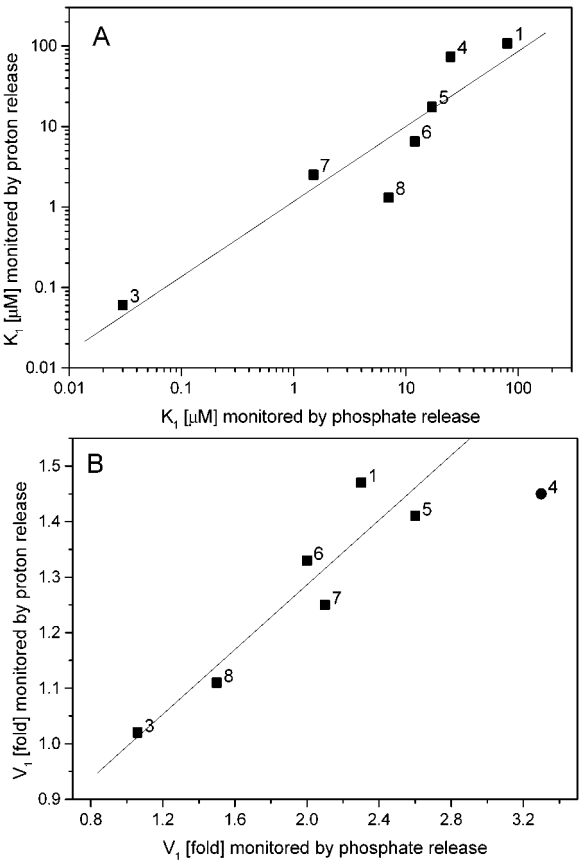

FIGURE 6: Correlation between the kinetic parameters (K_1 and V_1) determined from phosphate release measurements in plasma membranes vesicles formed of MDR1-transfected Chinese hamster ovary cells (CR1R12) and from measurements of ECARs of intact pig kidney cells (LLC-MDR1) by means of a Cytosensor microphysiometer. Compounds are numbered as in Table 1. (A) Concentrations of half-maximum activation, K_1, correlation coefficient $R = 0.935$, slope $m = 0.933$. (B) Maximum transporter activities, V_1, (if only activation occurred) $R = 0.935$, slope $m = 0.291$ [except for diltiazem (*4*) which shows an exceptionally high V_1 value in phosphate release measurements.]

LLC-MDR1) ≈ 1.6. We therefore conclude that the differences in kinetic constants V_i can be traced back to different expression levels of Pgp in the cell lines employed.

The excellent correlation between the fold velocities from proton and phosphate release measurements can be carried further to a quantitative analysis based on a net basal acidification rate of $\sim 1.3 \times 10^{-15}$ mol of H^+ min^{-1} $cell^{-1}$ for NIH-MDR-G185 cells and a Pgp content of ∼0.56 pg of Pgp/cell (*45*). For example, the verapamil (10 μM) induced 30% increase over the basal acidification in NIH-MDR-G185 cells leads to an extrusion rate of ∼0.69 μmol of H^+ min^{-1} $(mg\ of\ Pgp)^{-1}$. This is in good agreement with the rate of phosphate release [∼0. 4 μmol of P_i min^{-1} $(mg\ of\ Pgp)^{-1}$] upon stimulation of purified Pgp reconstituted in lipid membranes with the same amount of verapamil (*16*). It should, however, be noted that both values have to be considered as lower limits. Assuming one H^+ exported per ATP hydrolyzed, these calculations lead to an estimated ∼2 ATP molecules hydrolyzed for every verapamil molecule transported in NIH-MDR-G185 cells which is again in good agreement with previous estimations (*45*).

Pgp-Mediated Proton Translocation from the Cytoplasmic to the Extracellular Surface. The real-time pH measurements at the surface of MDR1-transfected cells demonstrate a linear correlation between the rate of intracellular phosphate release and extracellular proton extrusion upon drug-induced Pgp-ATPase stimulation. This correlation is likely to reflect a Pgp-mediated proton translocation from the site of ATP hydrolysis to the cell surface. Direct involvement of Pgp in proton translocation is further supported by (i) the direct correlation between the maximum rate of extracellular acidification, V_1, and the expression level of Pgp, (ii) the possibility to inhibit drug-stimulated proton translocation by cyclosporin A in a concentration dependent manner. The fact that other well-known pH regulators such as the Na^+/H^+ and the Cl^-/HCO_3^- exchanger are not involved in the process of extracellular acidification upon Pgp-ATPase activation points to the same direction. The same conclusion was drawn previously from indirect measurements using pH-sensitive dyes to monitor changes in the intracellular pH of Pgp overexpressing cells (*21*, *22*, *36*, *46*).

Possible Mechanisms of Proton Translocation form the Cytoplasmic to the Extracellular Membrane Surface. The quantitative correlation between extracellular proton release and intracellular phosphate release upon drug-induced Pgp-ATPase activation raises the question as to how protons are transported from the site of ATP hydrolysis at the cytoplasmic membrane surface to the outer cell surface. At least three possibilities can be envisaged: (i) A direct transport of protons by Pgp, (ii) a co-transport by exogeneous, or (iii) endogeneous substrates.

Most proton transporters known to date exhibit negatively charged groups in their transmembrane amino acid sequences (*47*). An analysis of the putative transmembrane sequences of Pgp based either on hydropathy plots (*11*, *12*) or on an amino acid sequence alignment of Pgp and the bacterial transporter MsbA (*5*) suggests that anionic residues are not located within the hydrophobic transmembrane sequences. Proton transport via acidic residues therefore seems unlikely. However, the transmembrane sequences of Pgp exhibit clusters of phenyl residues that might provide a slide guide for protons or cations (*12*).

Pgp has been shown to transport permanently charged cationic compounds (e.g., quarternary ammonium ions) provided these compounds reach the cytosolic side of the membrane (*48*, *49*). A transport of the charged form of drugs seems therefore possible. Many Pgp substrates carry cationic groups, which deprotonate during membrane diffusion but reprotonate when reaching the cytosolic side of the membrane. A proton co-transport with drugs appears thus to be possible. However, progesterone, which lacks a cationic group, also induces a strong increase in the ECAR. Whether this reflects a hydrogen bond interaction with one of the carbonyl groups of progesterone in the hydrophobic environment of the membrane remains to be tested. The fact that progesterone may even not be transported by Pgp renders this possibility rather unlikely.

A further possibility is a proton co-transport with an endogeneous substrate as suggested earlier (*22*). As mentioned above, lipids with phosphatidylcholine headgroups are possible endogeneous substrates (*12*, *50*). They possess a phosphatidic acid group with a $pK_a \sim 3$ in the lipid membrane and are thus in a nonprotonated form in the electrically neutral outer membrane surface (*51*). However, since the cytosolic membrane leaflet exhibits a negative surface potential and attracts protons from the bulk solution the lipid headgroups experience a pH which is about 2 orders of magnitude lower (*52*) than that of the bulk cytosol (∼pH 7). The ratio of protonated to unprotonated phosphatidic acid groups can thus be estimated as ∼1/100. The protonated form of phosphatidylcholine would thus be an ideal substrate for Pgp (*12*).

Conclusions. Using a microphysiometer, we have shown that Pgp-ATPase stimulation with drugs in intact cells is accompanied by changes in the ECAR . The good agreement between the rates of extracellular acidification and the rates of phosphate release in cellular vesicles establishes the microphysiometer method as a facile and precise technique to measure Pgp activation in living cells without the need for vesicle preparation.

ACKNOWLEDGMENT

We are grateful to Dr. P. Borst and Dr. M. M. Gottesman for generously providing transfected and wild-type cell lines and to Dr. S. V. Ambudkar for valuable advice in cell handling.

REFERENCES

1. Borst, P., and Schinkel, A. H. (1997) *Trends Genet. 13*, 217−22.
2. Ambudkar, S. V., Dey, S., Hrycyna, C. A., Ramachandra, M., Pastan, I., and Gottesman, M. M. (1999) *Annu. Rev. Pharmacol. Toxicol. 39*, 361−98.
3. Litman, T., Druley, T. E., Stein, W. D., and Bates, S. E. (2001) *Cell Mol. Life Sci. 58*, 931−59.
4. van Veen, H. W., Higgins, C. F., and Konings, W. N. (2001) *J. Mol. Microbiol. Biotechnol. 3*, 185−92.
5. Chang, G., and Roth, C. B. (2001) *Science 293*, 1793−800.
6. Raviv, Y., Pollard, H. B., Bruggemann, E. P., Pastan, I., and Gottesman, M. M. (1990) *J. Biol. Chem. 265*, 3975−80.
7. Romsicki, Y., and Sharom, F. J. (1999) *Biochemistry 38*, 6887−96.
8. Seelig, A., and Landwojtowicz, E. (2000) *Eur. J. Pharm. Sci. 12*, 31−40.
9. Chen, Y., Pant, A. C., and Simon, S. M. (2001) *Cancer Res. 61*, 7763−9.
10. Shapiro, A. B., and Ling, V. (1997) *Eur. J. Biochem. 250*, 122−9.

11. Seelig, A. (1998) *Eur. J. Biochem. 251*, 252−61.
12. Seelig, A., Blatter, X. L., and Wohnsland, F. (2000) *Int. J. Clin. Pharmacol. Ther. 38*, 111−21.
13. Sauna, Z. E., and Ambudkar, S. V. (2001) *J. Biol. Chem. 276*, 11653−61.
14. Sharom, F. J., Yu, X., Chu, J. W., and Doige, C. A. (1995) *Biochem. J. 308*, 381−90.
15. Litman, T., Zeuthen, T., Skovsgaard, T., and Stein, W. D. (1997) *Biochim. Biophys. Acta 1361*, 159−68.
16. Kerr, K. M., Sauna, Z. E., and Ambudkar, S. V. (2001) *J. Biol. Chem. 276*, 8657−64.
17. Ramachandra, M., Ambudkar, S. V., Chen, D., Hrycyna, C. A., Dey, S., Gottesman, M. M., and Pastan, I. (1998) *Biochemistry 37*, 5010−9.
18. Krupka, R. M. (1999) *J. Membr. Biol. 172*, 129−43.
19. Romsicki, Y., and Sharom, F. J. (2001) *Biochemistry 40*, 6937−47.
20. Raggers, R. J., Pomorski, T., Holthuis, J. C., Kalin, N., and van Meer, G. (2000) *Traffic 1*, 226−34.
21. Simon, S. M., and Schindler, M. (1994) *Proc. Natl. Acad. Sci. U.S.A. 91*, 3497−504.
22. Thiebaut, F., Currier, S. J., Whitaker, J., Haugland, R. P., Gottesman, M. M., Pastan, I., and Willingham, M. C. (1990) *J. Histochem. Cytochem. 38*, 685−90.
23. Roepe, P. D., Wei, L. Y., Cruz, J., and Carlson, D. (1993) *Biochemistry 32*, 11042−56.
24. Weisburg, J. H., Roepe, P. D., Dzekunov, S., and Scheinberg, D. A. (1999) *J. Biol. Chem. 274*, 10877−88.
25. Skovsgaard, T. (1990) in *Drug Resistance: Mechanisms and Reversal* (E, M., Ed.) pp 209−231, Libbey CIC, Rome.
26. Litman, T., Pedersen, S. F., Kramhoft, B., Skovsgaard, T., and Hoffmann, E. K. (1998) *Cell Physiol. Biochem. 8*, 138−50.
27. Chen, Y., and Simon, S. M. (2000) *J. Cell Biol. 148*, 863−70.
28. Altenberg, G. A., Young, G., Horton, J. K., Glass, D., Belli, J. A., and Reuss, L. (1993) *Proc. Natl. Acad. Sci. U.S.A. 90*, 9735−8.
29. Santai, C. T., Fritz, F., and Roepe, P. D. (1999) *Biochemistry 38*, 4227−34.
30. McConnell, H. M., Owicki, J. C., Parce, J. W., Miller, D. L., Baxter, G. T., Wada, H. G., and Pitchford, S. (1992) *Science 257*, 1906−12.
31. Parce, J. W., Owicki, J. C., Kercso, K. M., Sigal, G. B., Wada, H. G., Muir, V. C., Bousse, L. J., Ross, K. L., Sikic, B. I., and McConnell, H. M. (1989) *Science 246*, 243−7.
32. Litman, T., Zeuthen, T., Skovsgaard, T., and Stein, W. D. (1997) *Biochim. Biophys. Acta 1361*, 169−76.
33. Litman, T., Nielsen, D., Skovsgaard, T., Zeuthen, T., and Stein, W. D. (1997) *Biochim. Biophys. Acta 1361*, 147−58.
34. Schinkel, A. H., Wagenaar, E., van Deemter, L., Mol, C. A., and Borst, P. (1995) *J. Clin. Invest. 96*, 1698−705.
35. Cardarelli, C. O., Aksentijevich, I., Pastan, I., and Gottesman, M. M. (1995) *Cancer Res. 55*, 1086−91.
36. Hoffman, M. M., Wei, L. Y., and Roepe, P. D. (1996) *J. Gen. Physiol. 108*, 295−313.
37. Hollo, Z., Homolya, L., Davis, C. W., and Sarkadi, B. (1994) *Biochim. Biophys. Acta 1191*, 384−8.
38. Hafner, F. (2000) *Biosens. Bioelectron. 15*, 149−58.
39. Owicki, J. C., and Parce, J. W. (1992) *Biosens. Bioelectron. 7*, 255−72.
40. Dawson, R. M. C., Elliott, D. C., Elliott, W. H., and Jones, K. M. (1986) *Data for Biochemical Research*, 3rd ed., Clarendon, Oxford.
41. Hait, W. N., Stein, J. M., Koletsky, A. J., Harding, M. W., and Handschumacher, R. E. (1989) *Cancer Commun. 1*, 35−43.
42. Ayesh, S., Shao, Y. M., and Stein, W. D. (1996) *Biochim. Biophys. Acta 1316*, 8−18.
43. Hoffman, M. M., and Roepe, P. D. (1997) *Biochemistry 36*, 11153−68.
44. Hamilton, G., Cosentini, E. P., Teleky, B., Koperna, T., Zacheri, J., Riegler, M., Feil, W., Schiessel, R., and Wenzi, E. (1993) *Anticancer Res. 13*, 2059−63.
45. Ambudkar, S. V., Cardarelli, C. O., Pashinsky, I., and Stein, W. D. (1997) *J. Biol. Chem. 272*, 21160−6.
46. Robinson, L. J., and Roepe, P. D. (1996) *Biochem. Pharmacol. 52*, 1081−95.
47. Yerushalmi, H., and Schuldiner, S. (2000) *Biochemistry 39*, 14711−9.
48. Schmid, D., Ecker, G., Kopp, S., Hitzler, M., and Chiba, P. (1999) *Biochem. Pharmacol. 58*, 1447−56.
49. Smit, J. W., Weert, B., Schinkel, A. H., and Meijer, D. K. (1998) *J. Pharmacol. Exp. Ther. 286*, 321−7.
50. van Helvoort, A., Smith, A. J., Sprong, H., Fritzsche, I., Schinkel, A. H., Borst, P., and van Meer, G. (1996) *Cell 87*, 507−17.
51. Tocanne, J. F., and Teissie, J. (1990) *Biochim. Biophys. Acta 1031*, 111−42.
52. Beschiaschvili, G., and Seelig, J. (1992) *Biochemistry 31*, 10044−53.
53. Essodaigui, M., Broxterman, H. J., and Garnier-Suillerot, A. (1998) *Biochemistry 37*, 2243−50.

BI025720S